Membrane Properties of Principal Neurons of the Lateral Superior Olive

T. J. ADAM, P. G. FINLAYSON, AND D.W.F. SCHWARZ
The Rotary Hearing Centre, Department of Surgery (Otolaryngology), University of British Columbia, Vancouver, British Columbia V6T 2B5, Canada

Received 7 December 2000; accepted in final form 23 April 2001

Adam, T. J., P. G. Finlayson, and D.W.F. Schwarz. Membrane properties of principal neurons of the lateral superior olive. *J Neurophysiol* 86: 922–934, 2001. In the lateral superior olive (LSO) the firing rate of principal neurons is a linear function of inter-aural sound intensity difference (IID). The linearity and regularity of the "chopper response" of these neurons have been interpreted as a result of an integration of excitatory ipsilateral and inhibitory contralateral inputs by passive soma-dendritic cable properties. To account for temporal properties of this output, we searched for active time- and voltage-dependent nonlinearities in whole cell recordings from a slice preparation of the rat LSO. We found nonlinear current-voltage relations that varied with the membrane holding potential. Repetitive regular firing, supported by voltage oscillations, was evoked by current pulses injected from holding potentials near rest, but the response was reduced to an onset spike of fixed short latency when the pulse was injected from de- or hyperpolarized holding potentials. The onset spike was triggered by a depolarizing transient potential that was supported by T-type Ca^{2+}-, subthreshold Na^{+}-, and hyperpolarization-activated (I_H) conductances sensitive, respectively, to blockade with Ni^{2+}, tetrodotoxin (TTX), and Cs^{+}. In the hyperpolarized voltage range, the I_H, was largely masked by an inwardly rectifying K^{+} conductance (I_{KIR}) sensitive to blockade with 200 μM Ba^{2+}. In the depolarized range, a variety of K^{+} conductances, including A-currents sensitive to blockade with 4-aminopyridine (4-AP) and additional tetraethylammonium (TEA)-sensitive currents, terminated the transient potential and firing of action potentials, supporting a strong spike-rate adaptation. The "chopper response," a hallmark of LSO principal neuron firing, may depend on the voltage- and time-dependent nonlinearities. These active membrane properties endow the LSO principal neurons with an adaptability that may maintain a stable code for sound direction under changing conditions, for example after partial cochlear hearing loss.

INTRODUCTION

In the lateral superior olivary nucleus (LSO), inter-aural sound intensity differences (IIDs) within narrow frequency bands are linearly related to firing rate. This simple relationship appears to encode sound direction when measured over short poststimulus time periods in the tonotopically arrayed principal output neurons (Boudreau and Tsuchitani 1968; Caird and Klinke 1983; Finlayson 1995; Finlayson and Caspary 1993; Goldberg and Brown 1969). The linear relationship arises through an integration of excitatory and inhibitory synaptic inputs from the ipsilateral and contralateral ears. The excitatory input originates in glutamatergic spherical bushy cells of the ipsilateral ventral cochlear nucleus (VCN) (Cant and Casseday 1986; Glendenning et al. 1991). The inhibitory input is relayed from globular bushy cells in the contralateral VCN via glycinergic neurons in the medial nucleus of the trapezoid body (Cant and Casseday 1986; Glendenning et al. 1991; Moore and Caspary 1983; Spangler et al. 1985). The result of this integration is a highly regular discharge pattern of repetitive firing known as the "chopper response," where spikes are precisely timed in a train, as reflected in a multi-modal peristimulus time histogram (Goldberg and Brown 1969; Romand 1978; Tsuchitani 1982).

The regularity of the chopper response, also observed in VCN stellate cells (Pfeiffer 1966), has been attributed to diffuse synaptic inputs distributed along extensive dendritic arbors of these neurons (Rhode et al. 1983; Young et al. 1988a,b). Cable properties of the fine, long dendrites impose long time and space constants that transform brief synaptic current inputs into smooth, steady membrane polarization patterns (Rall 1989) and, hence, regular firing of action potentials. Indeed, excitatory postsynaptic responses to acoustic stimuli display slow depolarization levels (Finlayson and Caspary 1989), as expected from cable properties of the large dendritic arborizations of LSO neurons (Helfert and Schwartz 1987a,b; Scheibel and Scheibel 1974). The proposed passive role of the dendritic membrane in the integration of inputs should be reflected in linear membrane input/output relations. In models of VCN stellate neurons, it has been demonstrated that the chopper response is, in principle, compatible with linear voltage-current (*V-I*) relationships (Arle and Kim 1991; Banks and Sachs 1991; Hewitt and Meddis 1993). Linear *V-I* curves have, in fact, been reported for neurons recorded, in vitro, in the general region of the LSO (Wu and Kelly 1991, 1993).

Not all features of the principal LSO (pLSO) neuron are, however, easily reconciled with integration by passive cable properties alone. For example, the contralateral inhibitory input affects the membrane potential at the spike trigger zone through glycinergic synapses located at the soma and proximal dendrites (Glendenning et al. 1991; Spangler et al. 1985), compatible with short inhibitory postsynaptic potential (IPSP) rise times. In contrast, long excitatory postsynaptic potential (EPSP) rise times would be imposed by cable properties me-

Address for reprint requests: D.W.F. Schwarz, Dept. of Surgery/ENT, University of British Columbia, F153, 2211 Wesbrook Mall, Vancouver, British Columbia V6T 2B5, Canada (E-mail: dsch@interchange.ubc.ca).

The costs of publication of this article were defrayed in part by the payment of page charges. The article must therefore be hereby marked "*advertisement*" in accordance with 18 U.S.C. Section 1734 solely to indicate this fact.

diating the excitatory input directed, largely, to the dendritic periphery (Cant and Casseday 1986). LSO principal neurons must evaluate coincident excitation and inhibition over short time periods to detect, among other features, the movement of a sound source. We would expect, therefore, membrane mechanisms that are able to balance temporal aspects of the ipsilateral excitatory and contralateral inhibitory synaptic inputs. Thus nonlinear membrane properties may be required to account for the linear relation between IID and firing rate.

The short, invariant onset latency that is prerequisite for the multi-modal chopper response is not expected to emerge from EPSPs conducted passively from the dendritic periphery to the spike trigger zone. Long time constants and membrane potential fluctuations would be expected to impose long and variable latencies. In fact, in LSO principal neurons the onset emerges from a brief depolarizing transient potential, visible in subthreshold voltage responses to injected current pulses (Adam et al. 1997). The transient potential can be isolated from the spike by Na^+-current blockade with tetrodotoxin (TTX) and is followed, during maintained constant current, by a partial repolarization with a time course that is similar to the adaptation of spike rate in the chopper response. A parsimonious hypothesis would involve several voltage- and activity-dependent ion conductances in this response pattern. Responses to hyperpolarizing current pulse injections mirror the depolarizing responses: a transient peak hyperpolarization shortly after stimulus onset is followed by a voltage sag, back toward the resting potential, in spite of the continued hyperpolarizing current (Adam et al. 1997). Thus LSO neurons are equipped with special membrane properties that emphasize and balance the onset of both excitatory and inhibitory inputs. As a functional consequence of the onset emphasis, pLSO neurons are sensitive to the inter-aural time difference of low-frequency and amplitude-modulated sounds that cause a phase-locked firing pattern (Finlayson and Caspary 1991; Joris 1996; Joris and Yin 1995). The output signal depends, in magnitude, on the coincidence of inputs that would cause the peak de- and hyperpolarization in the subthreshold range.

The responses to injected current suggest active membrane behavior that involves a variety of voltage- and time-dependent conductances throughout the physiological voltage range of pLSO neurons. *V-I* relations may appear linear under such conditions, provided a balance exists between the magnitudes of conductances activated in the depolarized and hyperpolarized voltage ranges. This type of linearity should be limited to a narrow range of membrane potentials from which the de- and hyperpolarizing test currents are injected. Here, we report that the *V-I* relations of LSO principal neurons differ in linearity when tested from different membrane potentials, due to contributions by several voltage- and time-dependent conductances that have a prominent influence on the firing pattern.

METHODS

Long Evans rats, 9–16 days old, were deeply anesthetized with halothane and decapitated. A transverse brain stem block containing both LSO nuclei was quickly dissected in ice-cold artificial cerebrospinal fluid (ACSF) in which NaCl was replaced with sucrose. Using a Vibratome, we cut transverse brain stem slices, 300–350 μm thick, in the same solution and then transferred them to regular ACSF at 36°C. After an incubation period of 30 min, the slices were gradually cooled to 22°C and maintained at that temperature for up to 6 h before recording. The slices were then suspended on a nylon mesh in a recording chamber with a bath volume of 0.7 ml and perfused continually with ACSF at a rate of 4–6 ml per minute by means of a pump. The bath temperature was either 34 or 22°C. The conductances reported here were identified at either temperature, but we did not investigate temperature dependencies of their amplitudes or kinetics. The standard ACSF contained (in mM) 125 NaCl, 2.5 KCl, 2 $CaCl_2$, 2 $MgCl_2$, 1.25 NaH_2PO_4-H_2O, 10 D-glucose, and 25 $NaHCO_3$. After saturation with 95% O_2-5% CO_2 the pH was 7.3, and the osmolarity was 312 mOsm.

For whole cell recording we used patch pipettes pulled from borosilicate glass using a two-stage vertical puller (Narashige PP-83). The electrodes were filled with a solution containing (in mM) 115 K-gluconate, 20 KCl, 10 Na–*N*-2-hydroxyethylpiperazine-*N*-2-ethanesulfate (HEPES), 4 Mg-ATP, 0.3 Na-guanidine triphosphate (Na-GTP), 2 $CaCl_2$, and 10 ethylene glycol-bis (β-aminoethylether) *N*,*N*,*N*′,*N*′-tetraacetic acid (EGTA) to yield a calculated free Ca^{2+} concentration of 10^{-8} M (MaxChelator 1.2 software). Pipette resistance was between 5 and 8 MΩ. The electrode tips were placed on the slice surface within the LSO, as identified under a Zeiss dissection microscope, and advanced into the nucleus by means of a Newport micromanipulator system (actuator model 850B; controller PMC100). Cells were typically encountered between 50 and 150 μm from the tissue surface.

We used an Axoclamp 2B amplifier (Axon Instruments) in bridge mode to record membrane potentials and inject current, with optimal compensation for electrode resistance and capacitance. We offset the tip potential to zero in the bath fluid before recording and measured any deviation from zero after a session to extrapolate required corrections of the membrane potential, but we did not attempt to correct for further junction potentials. We low-pass filtered recorded data at 3 kHz, amplified them, and sampled at 20 kHz via National Instruments boards (MIO-16H; DMA-2800) in a MacIntosh Quadra 650 computer using A/Dvance software (McKellarDesigns).

Using electrophysiological criteria that distinguish the two types of morphologically identified LSO neurons in the rat (Adam et al. 1997), we selected LSO principal output cells for this report. Access for whole cell recording was obtained with seals of >1 GΩ. The neurons had overshooting action potentials, and membrane potentials were stable over recording sessions that generally exceeded 1 h. We measured voltage responses to 200-ms current pulses, injected through the recording electrode, from the resting membrane potential (RMP) or a different holding potential maintained with injected DC.

TTX was purchased from Tocris. All other chemicals and drugs were purchased from Sigma.

The experiments were approved by the Animal Care Committee of the University of British Columbia and conducted in compliance with the Canadian Guidelines for Animal Care.

RESULTS

Eighty-three neurons recorded in the LSO responded to constant supra-threshold current pulses, injected from rest, with highly regular trains of action potentials of short fixed onset latency. As shown in an earlier intracellular study (Adam et al. 1997), this behavior accounts for the multi-modal post-stimulus time histogram firing patterns of principal LSO neurons, with spike rates that rise with current intensity, mimicking "chopper responses" in the intact animal. Using whole cell recording techniques we now recorded RMPs of -62 ± 5.3 mV (mean ± SD), input resistances of 109 ± 64.4 MΩ, and membrane time constants of 8.5 ± 4.5 ms, measured at the offset voltage responses of <5 mV. The resistances and time constants were significantly greater than those recorded previously with intracellular (sharp) electrodes ($P < 0.01$) (Adam et

al. 1997). On depolarization beyond threshold, LSO principal neurons fired overshooting action potentials with amplitudes of 81.3 ± 15.3 mV and half-amplitude durations of 0.9 ± 0.6 ms.

Rectification in LSO principal neurons

Voltage responses in all principal LSO neurons displayed time- and voltage-dependent nonlinear relationships in responses to current pulses injected from rest or de- and hyperpolarized holding potentials. However, steady-state *V-I* relations measured just before pulse offset often showed only moderate rectification, particularly when determined at rest (Fig. 1, *B* and *E*) or a hyperpolarized holding potential (Fig. 1, *C* and *F*).

A depolarizing transient potential, visible in isolation in subthreshold depolarizing responses, triggered the first action potential (Fig. 1, *A–C*). While the transient potential varied in amplitude it increased, in all 83 neurons, on depolarization from negative holding potentials, suggesting contributions of conductances that are activated or de-inactivated in the hyperpolarized range. A contribution of strongly voltage-dependent inward conductances is suggested by an inflection in the rising phase of the transient potential in 58 neurons (Fig. 1, *B* and *C*). In all 83 neurons the transient potential was followed by a sustained outward rectification (Fig. 1), suggesting contributions to its decaying phase by outward currents activated in the depolarized range. Negative current pulses evoked hyperpolarizing peak potentials followed by a voltage sag back toward the RMP, resulting, within 100–150 ms, in a steady-state inward rectification that was most pronounced when measured from relatively positive holding potentials (Fig. 1, *A* and *D; n* = 83). This hyperpolarization-dependent inward rectification activated at approximately −60 mV, and approached a maximum at −70 to −80 mV. Thus hyperpolarization from such holding potentials evoked little or no sag. Inward currents activated in the hyperpolarized range likely account for this behavior.

Voltage dependence of action potential firing

We examined the influence of prevailing membrane potential on the firing pattern because synaptic inputs may occur, in vivo, during preexisting inhibition, and the "resting" membrane potential may vary, for example, as result of neuromodulation. In 25 neurons, we adjusted the amplitude of a test inward current pulse, injected from rest, to evoke a short train of action potentials. We then repeated the same stimulus immediately after a 200-ms prepulse that polarized the membrane to a value varied systematically between −50 and −110 mV (Fig. 2, *A* and *B*). The prepulse amplitude had only a small influence on the latency of the onset spike, which, presumably, was stabilized by the same conductances responsible for the transient potential. The latency (measured at the point the rising phase crossed 0 mV) was slightly shorter at rest than following hyper- or depolarization, resulting in a U-shaped function of the latency versus prepulse potential amplitude (Fig. 2*C; n* = 25). However, over a prepulse voltage range of −110 to −50 mV, the onset latency changed by only 3.2 ± 0.9 ms, or by 0.05 ms/mV. Thus the onset latency of a chopper

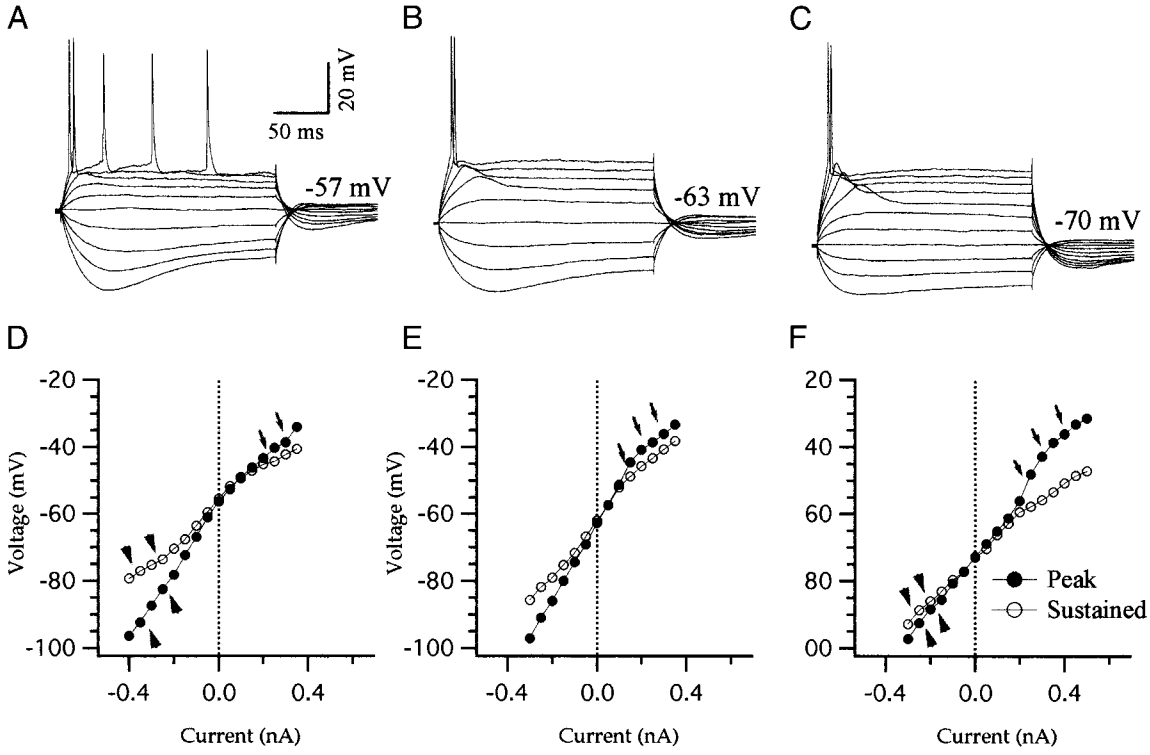

FIG. 1. Voltage-dependent nonlinearity of a principal lateral superior olive (LSO) neuron. *A–C*: voltage responses to equidistant current pulses injected from rest (*B*), a depolarized holding potential (*A*), and a hyperpolarized holding potential (*C*). *D–F*: current-voltage relations for the voltage responses above each graph. "Peak" data points (●) were measured at the subthreshold hyper- and depolarizing peaks, the "sustained" points at the end of the 200-ms pulse. The steady-state inward rectification is more pronounced when evoked from more positive holding potentials (arrowheads), the peak depolarization is greatest from hyperpolarized levels (arrows). All recorded principal LSO (pLSO) neurons displayed this pattern of nonlinear membrane behavior (*n* = 83).

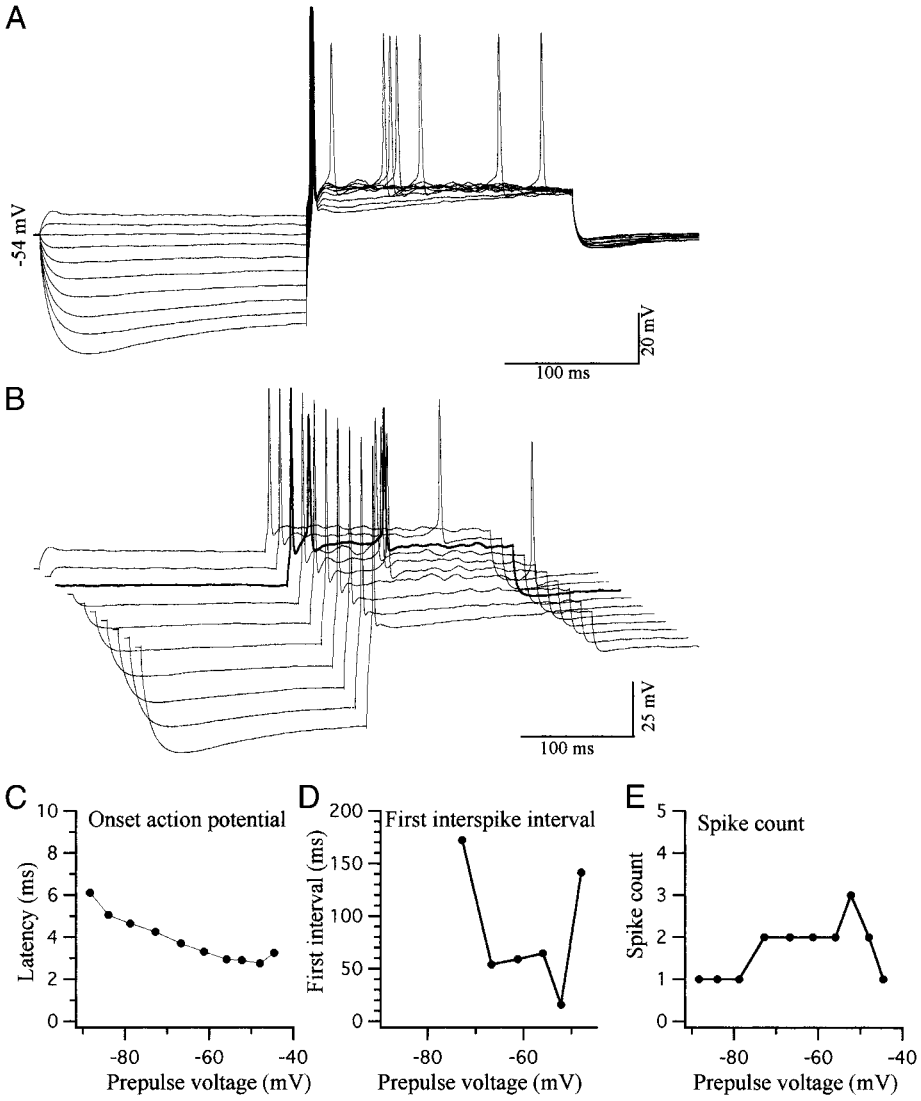

FIG. 2. Dependence of the firing pattern on the prestimulus membrane potential. Voltage responses to the same current pulse (200 ms), after prepulses to different potentials (step size ~4.5 mV), are shown superpositioned (*A*) and staggered (*B*). Note the restricted voltage range compatible with repetitive firing and voltage oscillations. Only the onset response is evoked from all membrane potentials. Onset latency is smaller at rest than at hyper- and depolarized prepotentials (*C*), as is the 1st interspike interval (*D*). The spike count is greatest at rest (*E*).

response is not very sensitive to the preexisting membrane potential.

In contrast, repetitive firing varied dramatically with the prepulse potential. In all 25 neurons tested with prepulses, we evoked repetitive firing from only a restricted range of prepotentials between approximately −50 and −70 mV (Fig. 2*B*). The highest spike counts were always evoked from rest, while fewer spikes were elicited in 16 neurons after prepolarization in either direction (Fig. 2*E*). In the remaining 9 of 25 neurons, repetitive firing could only be evoked from rest. Correspondingly, in 16 neurons the interval between the 1st 2 spikes was shortest when the test response arose from prepotentials close to rest (−50 to −55 mV) and longer from more negative or positive prepotentials (Fig. 2*D*).

Following prepolarization between approximately −70 and −50 mV, the test response was characterized by voltage oscillations that occurred after the onset action potential and triggered firing of further action potentials in 21 of 25 neurons (Fig. 2, *A* and *B*). These oscillations may actively support regularity of firing by maintaining firing times within the modes of the multi-modal chopper response, even after failure of individual action potentials (Adam et al. 1997). The oscillations faded in test responses evoked from negative prepotentials (less than −70 mV), being replaced by an extended spike afterhyperpolarization (AHP; Fig. 2*A*). In 18 of 21 neurons the magnitude of this AHP grew with the level of prehyperpolarization as expected from an outward conductance dependent on Ca^{2+} influx that is inactivated in the depolarized range. Thus prehyperpolarization tends to restrict firing to the onset spike, as observed in vivo when the excitatory ipsilateral response was preceded by inhibitory contralateral stimulation (Tsuchitani 1988a,b). Following predepolarization, firing after the onset spike was also suppressed, due, possibly, to a shunting action during the sustained outward rectification (Fig. 2*B*).

In summary, active membrane properties appear to guarantee short and precise onset latencies over a wide range of preexisting membrane potentials and support the multi-modal chopper response available from a narrower range of possible resting potentials.

Subthreshold Na^+ conductance

We characterized voltage-dependent conductances that account for the active nonlinear membrane behavior in LSO principal neurons. To study voltage-dependent nonlinearities independent of action potential firing, we applied the Na^+-

channel blocker, TTX (600 nM) in the ACSF. This application invariably hyperpolarized the RMP by a small amount (average: 3 mV), indicating that a persistent Na^+ conductance normally contributes to the resting potential of pLSO neurons. When testing membrane behavior at rest, we compensated for this hyperpolarization by DC injection. Due to its depolarization dependency, this voltage-activated conductance appears to contribute to the short stable onset latency and the transient potential (see *Conductances contributing to the transient potential* below).

Hyperpolarization-activated conductances

Injection of negative current pulses typically caused a hyperpolarizing peak, followed by a depolarizing sag of the membrane potential, despite a maintained current stimulus (Figs. 1–4). On hyperpolarization from rest, this voltage sag varied considerably in magnitude between neurons (compare Figs. 1*A* and 4*A*). Fifty-eight of the 83 neurons exhibited only slight sags, as in Fig. 4*A*. We hypothesized that a hyperpolarization-activated current, I_H, is responsible for the sag but is masked to varying extents by simultaneous activation of an inwardly rectifying potassium current, I_{KIR}, as in neurons of the auditory thalamus (Ströhmann et al. 1994; Tennigkeit et al. 1996).

In the presence of TTX, we first evoked the voltage sag on hyperpolarization (Fig. 3*A*) and then applied Ba^{2+} to the bath at a concentration that selectively blocks the inward rectifier (0.2 mM) (Nichols and Lopatin 1997). Barium application depolarized the membrane by 7.2 ± 2.2 mV ($P < 0.01$), increased the input resistance by 61.8 ± 29.9% ($P < 0.01$), and raised the slope resistance in the hyperpolarized range, measured at the peak, by 77 ± 23.6% (Fig. 3*D; n* = 7/7). Thus Ba^{2+} application greatly increased hyperpolarization amplitudes, mainly of the peak, but also at steady state (Fig. 3, *B* and *D*), suggesting a strong contribution of I_{KIR} to the membrane conductance in the hyperpolarized range. In all seven neurons the depolarizing sag in hyperpolarizing responses was markedly enhanced in the presence of Ba^{2+}, presumably due to unmasking of the gradually activating I_H by I_{KIR} blockade. In the voltage range of a well-developed sag (negative to approximately −65 mV), the slope resistance was not significantly increased by Ba^{2+} (Fig. 3*E; n* = 7/7), illustrating a major role of the remaining I_H in the membrane conductance.

Application of the I_H blocker, Cs^+ (3 mM; $n = 6$), to the ACSF (in addition TTX and Ba^{2+}) completely eliminated the sag ($n = 6/6$). Cs^+ increased the membrane resistance, measured close to the RMP, by 170.1 ± 3.3% ($P < 0.01$) and the slope resistance in the hyperpolarized range by 482 ± 176% ($P < 0.01$; cf. Fig. 3*E*). These values were low estimates as strong hyperpolarizations were incomplete at the end of the 200-ms pulse due to greatly prolonged time constants (Fig. 3*C*). The Cs^+-induced increase in resistance (Fig. 3*E*) suggests that I_H normally dominates the conductance in the hyperpolarized range in pLSO neurons. Furthermore, the Cs^+ application hyperpolarized the RMP by 5.0 ± 2.1 mV, indicating that I_H contributes to the RMP. The slow deactivation of the I_H after termination of hyperpolarizing pulses led to a transient depolarizing afterpotential (Fig. 3*B*, arrowhead) that could serve to emphasize the onset of a response to depolarization (e.g., an EPSP) from negative potentials or rest in a voltage-dependent manner. Thus the strong expression of I_H, and its masking by I_{KIR}, may be of great functional importance.

Conductances contributing to the transient potential

In many respects, the depolarizing afterpotential following a hyperpolarizing pulse was similar to the transient potential. Both increased with the magnitude of hyperpolarization of a pulse or the prevailing holding potential (Figs. 1 and 3–5), and both were greatly amplified after application of Ba^{2+} (Figs. 3*B*, 4*B*, and 5*B*). An increase in amplitude under Ba^{2+} was expected as a consequence of K^+ channel blockade (raised resistance); however, a greater permeability of Ca^{2+} channels to

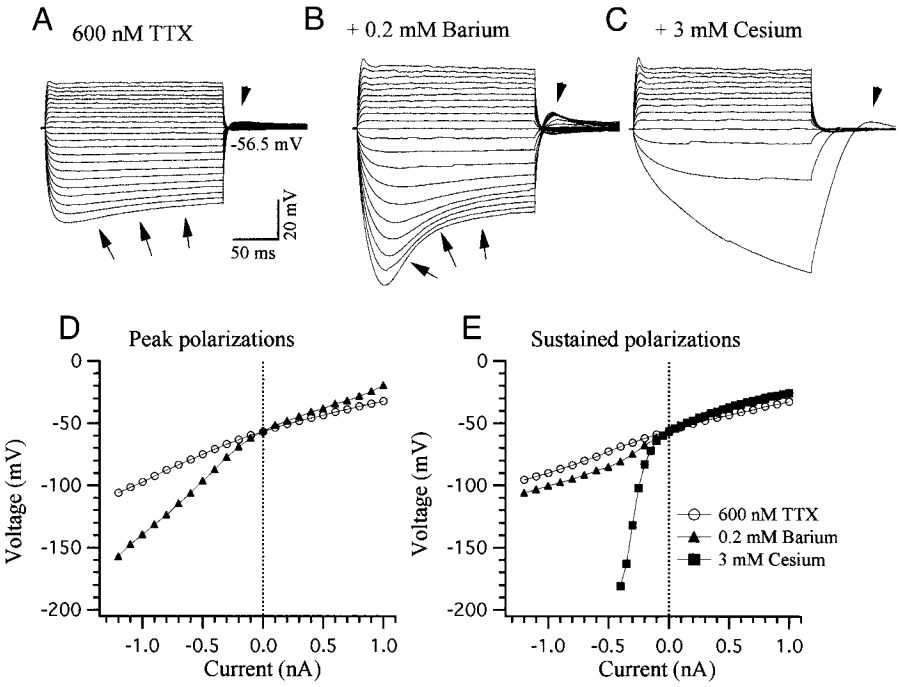

FIG. 3. Hyperpolarization-activated conductances. *A*: a moderate voltage sag in hyperpolarizing responses to current pulses (arrows), and a weak, transient postpulse depolarizing afterpotential (arrowhead), are seen in the presence of TTX (600 nM). *B*: blockade of I_{KIR} with 0.2 mM Ba^{2+} greatly amplifies the peak hyperpolarization and depolarizing afterpotential and unmasks most of the sag. *C*: additional blockade of I_H with 3 mM Cs^+ greatly raises hyperpolarizing voltage responses, and eliminates the sag, as well as most of the depolarizing afterpotential. *D*: Ba^{2+} application raises peak slope resistance much more on hyperpolarization than depolarization. *E*: changes in steady-state resistance on Ba^{2+} application are smaller and restricted to the voltage range below approximately −60 to −70 mV. Blockade of I_H with Cs^+ causes a large increase in slope resistance throughout the hyperpolarized range.

Ba^{2+}, compared with Ca^{2+}, could also contribute (Huguenard 1996). We investigated a possible contribution of the transient Ca^{2+} current, I_T, to the depolarizing afterpotential and transient potential. We evoked depolarizing afterpotentials, following hyperpolarization from rest, in the presence of TTX (600 nM) to block any contamination by action potential firing (Fig. 4*A*). After an amplification of the depolarizing afterpotential with Ba^{2+} (0.2 mM; Fig. 4*B*), we applied Cs^+ (3 mM; Fig. 4*C*) to remove the large contribution of I_H to the depolarizing afterpotential. We then added the T-channel blocker, Ni^{2+} (50 μM; Fig. 4*D*) to the ACSF. The result was an almost complete elimination of the depolarizing afterpotential, consistent with a contribution by a transient Ca^{2+} current, I_T ($n = 5$).

The transient potential displayed qualitatively similar behavior. We depolarized the neurons ($n = 7$) from a holding potential of approximately −80 mV (deinactivating T-type currents) and evoked transient potentials in the presence of TTX (Fig. 5*A*). Again, the transient potentials were greatly amplified after addition of 0.2 mM Ba^{2+} to the bath (Fig. 5, *B* and *C; n* = 7/7). An addition of Cs^+ (3 mM) then removed the I_H contribution to the transient potential, which now occurred with longer and more variable latencies (Fig. 5, *D* and *G; n* = 6/6). Paradoxically, the net amplitudes were raised in the presence of Cs^+, presumably due to a great increase in impedance caused by the I_H blockade. Subsequent co-application of Ni^{2+} eliminated the transient potential and thus reduced the depolarizing peak potentials (Fig. 5*F*), but for a small emphasis of the depolarization onset (Fig. 5*E; n* = 5/5). Therefore I_T seems to contribute to the transient potential, although its short and relatively constant latency depends on activation of an I_H.

We characterized the role of Ca^{2+} influx by comparing voltage responses, including the depolarizing afterpotential and transient potential, measured after a 10-fold reduction of the Ca^{2+} concentration and in standard ACSF ($n = 8$). The depolarizing afterpotential, evoked in the presence of 2 mM Ca^{2+} (and TTX), was reduced in amplitude and duration in medium containing only 200 μM Ca^{2+} (Fig. 6; $n = 8/8$). Thus a Ca^{2+} influx seems to contribute to the transient depolarization for a longer period of time than the decaying I_H. In contrast, a blockade of the I_H with Cs^+ led to prolonged (up to 100 ms) and variable latencies of the Ca^{2+}-dependent depolarizing afterpotentials (e.g., Fig. 4*C; n* = 6). Apparently, the I_H is largely responsible for the constant short onset latencies of depolarizing responses from hyperpolarized potentials (e.g., Fig. 2).

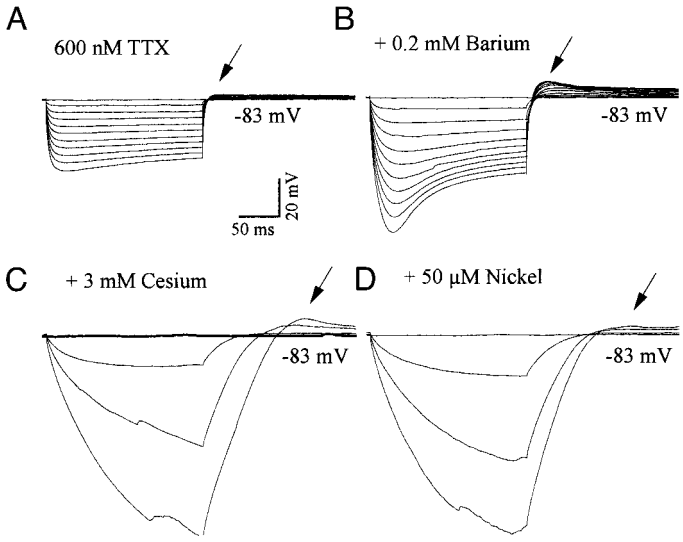

FIG. 4. Contribution of I_T to the postpulse depolarization. Small depolarizing afterpotentials following a weak sag in the presence of TTX (*A*, arrow) are amplified by application of Ba^{2+} (*B*). The depolarizing afterpotential remaining after additional I_H blockade with Cs^+ is greatly reduced after blockade of I_T with 50 μM of Ni^{2+} (*D*).

A Ni^{2+}-sensitive depolarizing conductance, activating between approximately −70 and −55 mV, appeared to make a large contribution to the amplitude of the transient potential (Fig. 5, *B, E,* and *F*). Despite the limited selectivity of the Ni^{2+} blockade, this relatively negative voltage range of activation suggested a strong contribution of a transient (T-type) Ca^{2+} conductance. As a confirmation, we compared depolarizations evoked from negative holding potentials (−75 mV) in standard TTX containing ACSF with and without 50 μM of Ni^{2+} ($n = 7$). Nickel application strongly reduced the amplitudes of the transient potential (peak depolarization in Fig. 7, *A* and *C*) but also diminished the steady-state depolarization to a lesser degree (Fig. 7*D; n* = 7/7). This effect is consistent with a contribution of a transient Ca^{2+} current but does not exclude participation of other conductances, particularly at depolarized levels. In the absence of TTX, Ni^{2+} application (50 μM) raised the current intensities required to trigger an action potential from hyperpolarized holding potentials (−75 mV in Fig. 7*D; n* = 5/5). No significant increase in current was required, however, to evoke action potentials from holding potentials positive to −60 mV. Therefore a Ni^{2+}-sensitive Ca^{2+} current that is inactivated at −60 mV seems to have a major role, in concert with I_H, in the latency stabilization of onset spikes evoked from a hyperpolarized voltage range (cf. Fig. 2).

A Na^+ current contributes to the RMP of LSO principal neurons, as an application of TTX (300–600 nM) caused a hyperpolarization (3 ± 0.4 mV) in 14/14 neurons. We compensated for the TTX-induced hyperpolarization with depolarizing current (e.g., to the original RMP of −58 mV in Fig. 8*A*) to measure voltage responses to hyper- and depolarizing current pulses under comparable conditions before and after TTX application. The *V-I* relations of the hyperpolarizing responses were identical; however, the slope of the *V-I* curves representing the peak depolarization decreased by 41.3 ± 10.2% in the voltage range between the RMP and firing threshold as a consequence of TTX application (Fig. 8*C*). We repeated the same type of measurements from hyperpolarized holding potentials (e.g., −73 mV in Fig. 8, *D–F*) and obtained TTX-reduced subthreshold depolarization amplitudes in a similar voltage range. In about one-half of the neurons ($n = 6/14$), steady-state depolarizations measured at the end of the 200-ms pulse were also reduced by TTX application, documenting the blocked depolarizing effect of a long-lasting Na^+ conductance. Thus a non- or slowly inactivating, subthreshold Na^+ conductance contributes to depolarization amplitudes above approximately −60 mV, potentially accelerating the onset response. It remains to be elucidated which TTX-sensitive Na^+ channels account for the Na^+ conductance at different voltage levels in principal LSO neurons.

Depolarization-activated K^+ conductances

In spite of contributions by a persistent Na^+ conductance, the decaying phase of the transient potential may be explained,

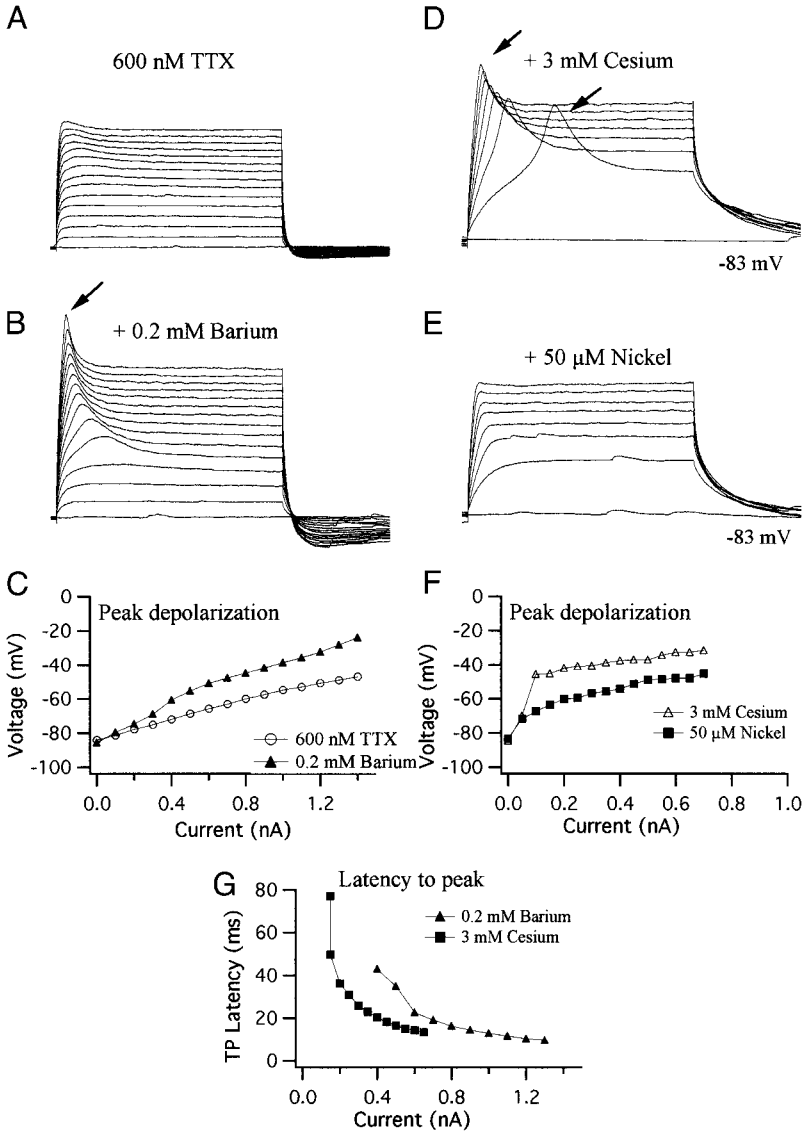

FIG. 5. Conductances contributing to the transient potential (TP). *A*: a small transient potential is evoked, from a hyperpolarized holding potential (−83 mV), in the presence of TTX. *B*: blockade of the I_{KIR} with 0.2 mM Ba^{2+} amplifies the transient potential (arrow). *C*: Ba^{2+} application causes an increase in slope resistance, mainly negative to 60 mV. *D* and *G*: additional blockade of I_H with Cs^+ prolongs the latency of the transient potential. *E*: T-current blockade with Ni^{2+} eliminates the transient potential. *F*: Ni^{2+} application attenuates the transient peak depolarization over a narrow stimulus intensity range, consistent with blockade of a low-threshold Ca^{2+} spike (LTS).

to a large extent, by the decline of the transient I_T, I_H, and, possibly, subthreshold I_{Na}. We hypothesized a further contribution of depolarization-activated K^+ currents because of an increase in rate of the transient potential decay with depolarization amplitude (e.g., Fig. 1). We therefore compared voltage responses before and after K^+ channel blockade. Application of 4-aminopyridine (4-AP), a blocker of transient K^+ currents (McCormick 1991), produced a concentration-dependent depolarization of the resting potential in the presence of TTX (300–600 nM; $n = 7$). For example, 1 mM of 4-AP changed the RMP from −62.7 ± 2.7 mV to −42.0 ± 5.7 mV, and 4 mM to −38.5 ± 4.9 mV. 4-AP–sensitive outward currents are therefore at least partially activated at rest. However, 50 and 200 µM 4-AP did not significantly alter the RMP. These lower concentrations led to an increase in voltage amplitude during and immediately after the transient potential, evoked from hyperpolarized holding potentials (Fig. 9*A*), and to enlarged depolarization amplitudes early during a pulse elicited from holding potentials close to rest (Fig. 9*B*). *V-I* relations showed that the low 4-AP concentrations led to amplitude increases of the initial portions of depolarizing responses above approximately −50 mV, as shown for the voltage sag (arrow in Fig. 9*A*) immediately following the transient potential in Fig. 9*C*. Steady-state responses measured at the end of the pulses were unaffected by 50 µM 4-AP (Fig. 9*D*). Higher 4-AP concentrations (1–4 mM) were required to elevate steady-state depolarizations (not shown). These data are compatible with a selective blockade of transient A-type K^+ currents by low

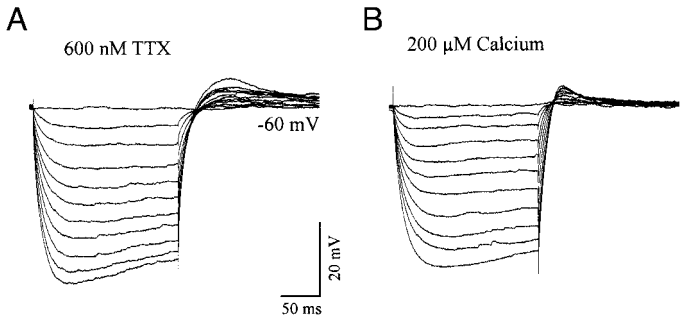

FIG. 6. Depolarizing afterpotentials following hyperpolarizing pulses in the presence of TTX (*A*) were reduced in amplitude and duration after a tenfold reduction of extracellular [Ca^{2+}] (*B*).

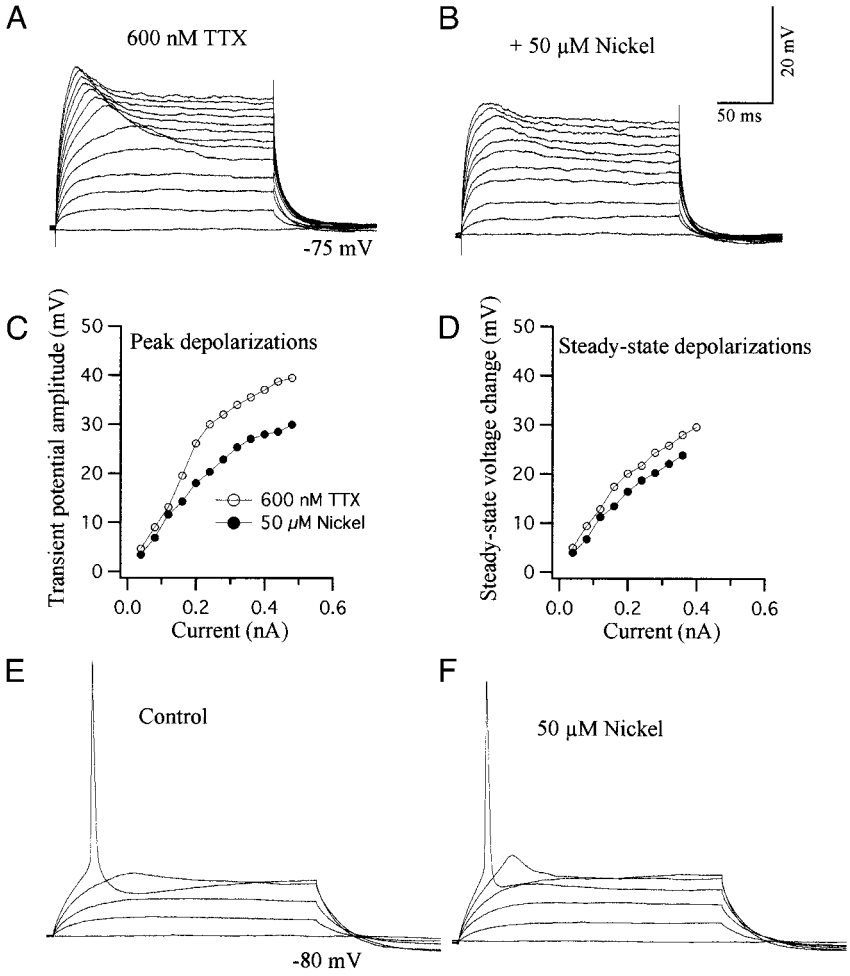

FIG. 7. The contribution of the LTS to the transient potential and onset discharge. Depolarizing pulses from a hyperpolarized potential (−75 mV) evoked transient potentials in the presence of TTX (*A*) that were reduced by Ni^{2+} application (*B; n* = 7/7). The Ni^{2+}-induced reduction of the voltage amplitude was pronounced during the peak (*C*) but also present to a modest degree at the end of the pulse (*D*). When TTX was omitted from the medium depolarizing pulses from −80 mV evoked an onset spike with lower current intensities in control ACSF (*E;* 0.22 nA) than after application of Ni^{2+} (*F;* 0.34 nA).

4-AP concentrations (McFarlane and Cooper 1991; Storm 1990) and illustrate an additional contribution of sustained K^+ currents, sensitive to higher 4-AP concentrations, to depolarizing responses and the RMP.

Activation of an A-type K^+ current would be expected to accelerate the rate adaptation in a neuron's discharge pattern during depolarization. To investigate this possibility we applied 50 μM of 4-AP without TTX (n = 6). At higher 4-AP concentrations we were unable to maintain stable recording conditions, due to excessive spontaneous firing. A single onset spike response evoked, from rest or hyperpolarized holding potentials, by a threshold current pulse amplitude under control conditions was transformed into sustained repetitive firing after application of 50 μM 4-AP (Fig. 10). Suprathreshold depolarization from rest that resulted in a short, strongly adapting spike burst in control ACSF also caused sustained firing with very little, if any, adaptation in the presence of 4-AP (Fig. 10). Spike amplitudes and durations were also magnified after application of 4-AP. Therefore A-type K^+ currents expressed in pLSO neurons accelerate the decay of action potentials and contribute strongly to the spike rate adaptation that normally characterizes the chopper response.

Transient outward currents cannot explain the sustained depression of depolarization following the transient potential (e.g., Figs. 1 and 5*B*), although the sustained current sensitive to high 4-AP concentrations could. We considered contributions of further depolarization-activated K^+ currents and applied the broad spectrum K^+-channel blocker, tetraethylammonium (TEA) in ACSF containing 600 nM TTX (n = 6). At concentrations between 5 and 30 mM, TEA had no significant effect on the RMP. However, voltage responses to depolarizing pulses were strongly amplified in the presence of 5 mM TEA, both early and late during the pulse (Fig. 11, *A* and *B*). At higher concentrations (20 mM in Fig. 11*C*) a depolarizing ramp potential led, in addition, to a peak at a long and variable latency during small current pulses. At higher stimulus intensities the ramp triggered an all-or-nothing spike at an inflection point of approximately −35 mV. After a broad peak, this high-threshold spike (HTS) terminated in a plateau depolarization that lasted throughout the duration of the pulse and some times longer (Figs. 11*C* and 12*C*). *V-I* relations for depolarizations from rest (−61 mV in Fig. 11) demonstrate a linear increase in response amplitude at 5 mM but, at 20 mM, a sudden strong increase in slope at approximately −35 mV, reflecting the HTS early, and the plateau late in the response (Fig. 11, *D* and *E*). Thus TEA blockade of a sustained K^+ conductance that does not normally contribute to the RMP unmasked a regenerative depolarizing process capable of producing HTSs with plateaus.

We assessed the influence of the TEA-sensitive conductance on the firing pattern by recording depolarizing responses without TTX in the ACSF (n = 6). As a precaution against excessive firing, we injected positive current pulses from a holding potential of −80 mV, evoking, above threshold, a

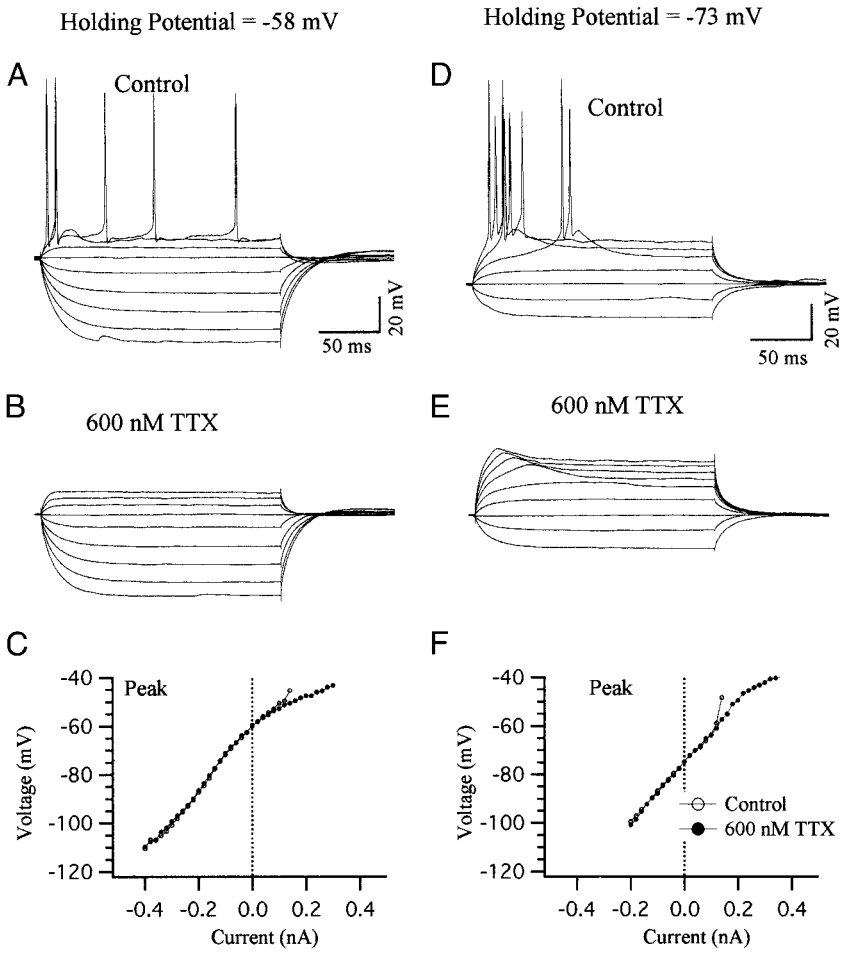

FIG. 8. A subthreshold Na^+ conductance supports the onset response. The peak subthreshold depolarization, evoked from rest, was greater under control conditions (*A* and *C*, ○) than after TTX application (*B* and *C*, ●; $n = 14/14$). In this neuron the TTX effect was only evident in a small voltage range depolarized from rest (*C*). A similar behavior was evident when depolarizing pulses were injected from a hyperpolarized holding potential (*D–F*). Note that the suprathreshold discharge was restricted to a brief onset burst when evoked from the hyperpolarized holding potential (*D*), whereas repetitive firing was evoked from rest (*A*).

single onset spike under control conditions (Fig. 12*A*, cf. Fig. 2). Addition of 5 mM TEA to the ACSF transformed this pattern. At suprathreshold stimulus intensities, repetitive firing of spikes, with gradually increasing amplitudes and durations, occurred after the onset action potential, which, at moderate current strengths, was followed by a brief pause in firing (Fig. 12*B*). The action of A-type currents, not blocked by TEA, probably prevented spike discharge during the pause. After application of 20 mM TEA the onset spike led, without repolarization, to a plateau potential (Fig. 12*C*), caused, presumably, by blockade of repolarizing K^+ currents (Storm 1987). A brief, negative voltage sag between onset spike and plateau may also have been caused by A-current activity.

Mechanisms supporting the high-threshold spike

We never observed an HTS under control conditions, but they commonly occurred after application of high TEA concentrations (e.g., 20 mM in Figs. 11*C*, 12*C*, and 13*B*). Since they are readily evoked in the presence of TTX, we assumed that a Ca^{2+} current accounted for both HTSs and plateaus. We confirmed this assumption as follows: In the presence of TTX we first recorded voltage responses to depolarizing current pulses under control conditions (Fig. 13*A*) and then applied 20 mM TEA. After establishing current pulse amplitudes that reliably evoked HTSs and plateaus (Fig. 13*B*), we applied Cd^{2+} at a concentration (50 μM) that selectively blocks high-threshold Ca^{2+} currents in other neurons (Huguenard 1996). On repetition of the depolarizing pulses, we found that the presence of Cd^{2+} completely prevented firing of the HTSs and plateaus (Fig. 13*C*). Low-threshold Ca^{2+} spikes and transient potentials evoked from hyperpolarized potentials were not affected by application of 50 μM Cd^{2+} (not shown). We also compared Ca^{2+} spikes in control ACSF (2 mM Ca^{2+}) and after reduction of the Ca^{2+} concentration to 200 μM ($n = 5$). This reduction of the external Ca^{2+} concentration eliminated the neuron's ability to fire either HTS or LTS and reduced the amplitude of the transient potential (cf. Fig. 6). These data show that LSO principal neurons are equipped with at least two pharmacologically distinct Ca^{2+} conductances, a Ni^{2+}-sensitive transient low-threshold conductance that accounts for LTS and amplifies the transient potential, and a high-threshold conductance able to support HTSs and sustained plateaus.

DISCUSSION

Principal neurons in the LSO are thought to extract information about sound direction by combining the excitatory input from the ipsilateral ear with the contralateral inhibitory input. A regular firing pattern and smooth depolarization recorded at the soma during acoustic stimulation have led to the assumption that both inputs are integrated by cable properties of the large dendritic tree. Given normal fluctuations in membrane potential, this passive integration model would have difficulty accounting for the temporal firing pattern of pLSO neurons. In particular, this model is incompatible with the

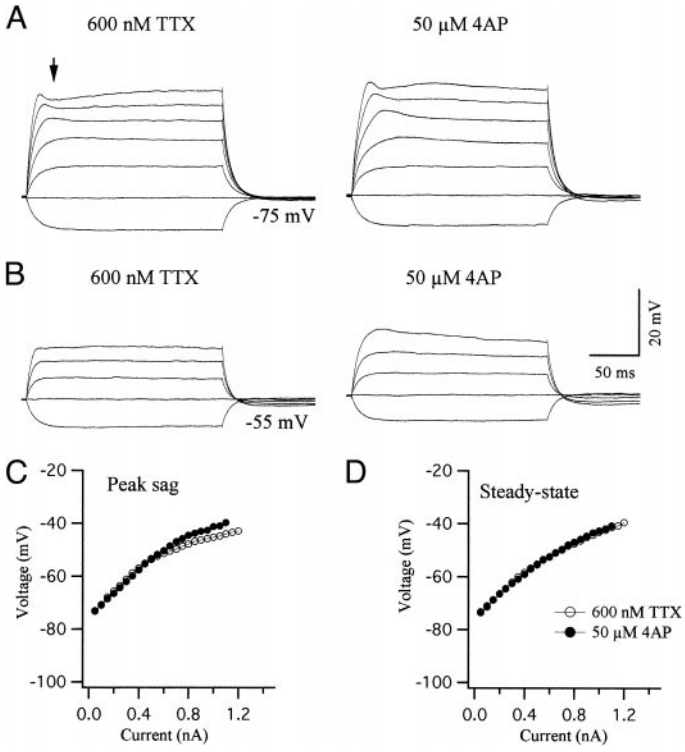

FIG. 9. A-type K^+ current reduces amplitudes of early depolarizing responses. *A*: application of 50 μM 4-aminopyridine (4-AP) led to an amplitude increase early in depolarizing responses evoked from a hyperpolarized holding potential. *B*: a similar amplitude increase was observed on depolarization from potentials near rest. *C*: the amplitude increase occurred in a voltage range depolarized above approximately −50 mV (holding potential: 75 mV). *D*: amplitudes at the end of the 200-ms pulse were not affected by 50 μM 4-AP (holding potential: 75 mV).

narrow range of onset latencies that is prerequisite for the chopper response. Active membrane properties appeared necessary to explain the firing pattern.

Here, we present evidence for a rich complement of voltage- and time-dependent conductances, which are expected to

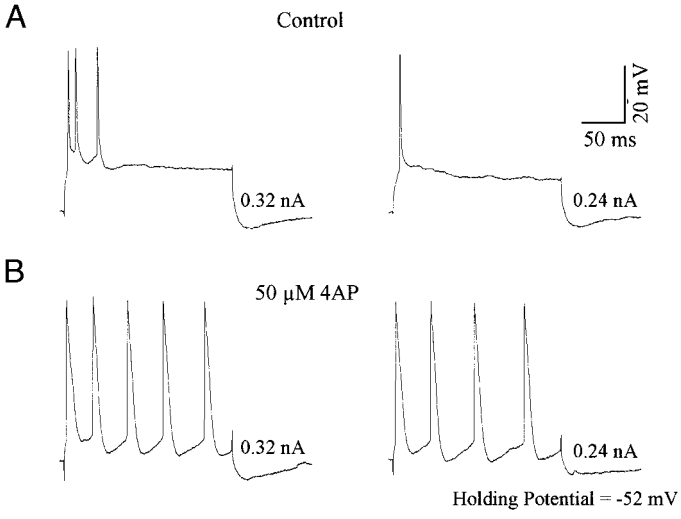

FIG. 10. An A-type current contributes a spike rate adaptation. *A*: in standard artificial cerebrospinal fluid (ACSF) depolarization from −52 mV leads to a single onset action potential at threshold (*right*) and to a strongly adapting brief burst at suprathreshold current strength (*left*). Responses to stimuli of the same strengths are transformed into regular repetitive firing with broadened spikes after application of 50 μM 4-AP.

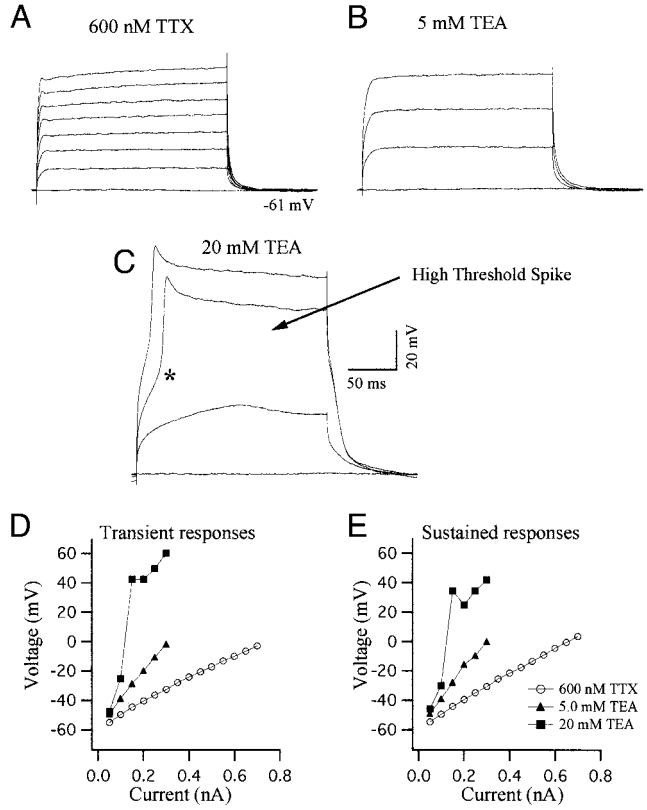

FIG. 11. A sustained, tetraethylammonium (TEA)-sensitive K^+ conductance is present in LSO principal neurons. *A*: in the presence of TTX, depolarizing responses to current pulses injected from rest consist of a small initial transient potential and consecutive steady depolarization levels. Both early (*D*) and sustained responses (*E*) have a near linear relationship with current intensity. *B*: voltage amplitudes are magnified after application of 5 mM TEA, leading to an increase in apparent slope resistance (*D* and *E*). *C*: application of 20 mM TEA enabled a regenerative depolarizing process expressed as positive ramp leading to a peak at low depolarizing currents and a high-threshold spike (HTS) triggered at approximately −35 mV (*), followed by a plateau, at higher intensity. The HTS and plateau are responsible for a sudden increase in apparent slope resistance measured at the peak (*D*) and termination of the pulse (*E*), respectively.

strongly affect the integration of postsynaptic potentials at the spike trigger zone and shape the pattern of output firing. Apart from the mechanisms for action potential generation, LSO neurons exhibit many voltage-dependent conductances that activate on depolarization, including a subthreshold Na^+, low- and high-threshold Ca^{2+} currents, and 4-AP– and TEA-sensitive K^+ currents. In addition, two distinct conductances, I_H and I_{KIR} are activated during hyperpolarization.

Principal neurons of the LSO transform the firing patterns of excitatory and inhibitory input fibers, which are similar to auditory nerve ("primary-like") responses, into a new signal termed the chopper response. This multi-modal firing pattern characterizes pLSO neuron responses to tonal stimuli, in vivo, and to current injection in tissue slices. Temporal and spatial integration of excitatory input at the periphery of the extensive dendritic tree probably accounts for much of the prerequisite regularity. However, the combination of inward and outward conductances activated on depolarization contributes a strong current shunt that will attenuate voltage fluctuations, promoting regularity. Furthermore, active membrane properties, albeit unidentified, must be responsible for the voltage oscillations that appear, in response to injected current pulses, at times of

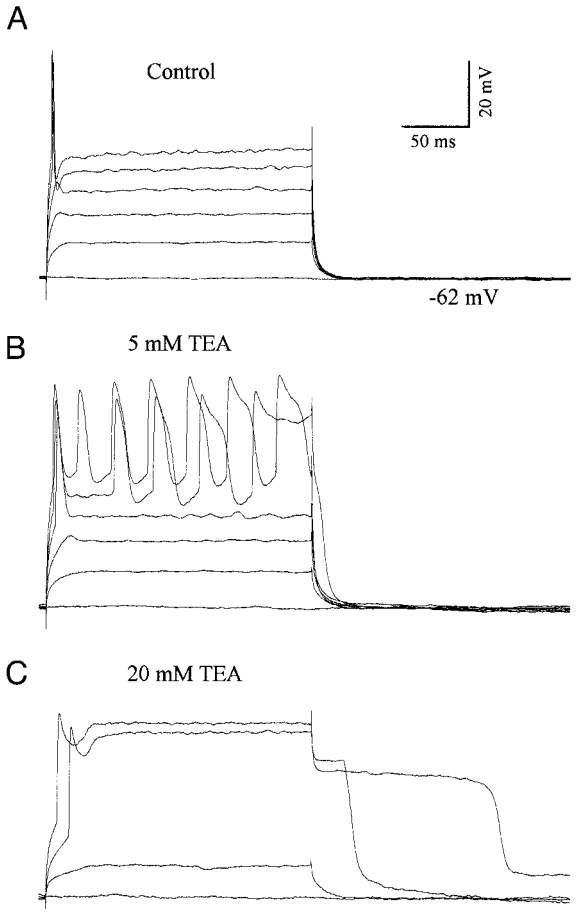

FIG. 12. Blockade of a TEA-sensitive K^+ conductance transforms an onset response into repetitive firing. *A*: depolarizations evoked a single onset spike. *B*: application of 5 mM TEA enabled repetitive firing with spikes of gradually increasing amplitude and width. *C*: after application of 20 mM TEA firing of action potentials was prevented by depolarizing plateau potentials that exceeded the duration of the stimulus pulse.

failed action potentials or after cessation of firing (Adam et al. 1997; Fig. 2, *A* and *B*). We believe that these oscillations also support regularity. It is certainly not true that the regularity simply reflects passive linear membrane behavior, since voltage-activated conductances cause different degrees of nonlinearities in input/output relations at different preexisting membrane potentials (Fig. 1).

Both input and output firing patterns share an emphasis of stimulus onset. However, the onset emphasis is not simply imported from the excitatory synaptic input. Active membrane properties of the output neurons amplify the response onset as evident in the transient potential. I_T, I_H, I_{Na}, and A-type currents contribute to the transient potential. Their magnitudes vary with the preexisting membrane potential, due to different activation voltage ranges. During ipsilateral excitation, in vivo, subthreshold Na^+ and transient Ca^{2+} currents will accelerate depolarization and shorten the onset latency, in spite of long dendritic time constants. These nonlinear properties temporally fix the onset of the regular firing pattern at a short latency, enabling the multi-modal chopper response. Thus the low-pass filter properties of the long dendrites are largely compensated by intrinsic voltage- and time-dependent membrane conductances. 4-AP– and TEA-sensitive K^+ conductances repolarize and shunt the membrane after the transient potential. They serve, therefore, as intrinsic mechanisms for spike rate accommodation. Since onset emphasis and adaptation are actively maintained, they probably are of critical importance for the output code of the LSO.

A hyperpolarization of the membrane potential has been recorded in pLSO neurons during inhibitory contralateral acoustic stimulation (Finlayson and Caspary 1989). The extent of this glycinergic hyperpolarization depends on the equilibrium potential for chloride (E_{Cl}) and the activation of voltage-dependent conductances in the negative voltage range, e.g., I_{KIR} and I_H. Reversal potentials of glycine-evoked IPSPs have been measured at -73.0 ± 7.1 mV in the LSO of rat pups, aged 10 days or more, with micropipettes containing 2 M K-acetate (Kandler and Friauf 1995). As this technique imposes a negative bias on the E_{Cl}, the chief inhibitory effect of the glycinergic contralateral input may be a powerful shunt conductance at the proximal soma-dendritic membrane, between the dendritic periphery (receiving excitation) and the spike trigger zone, rather than hyperpolarization. What then, is the role of the hyperpolarization-activated currents?

The activation kinetics of the two hyperpolarization-activated currents, I_H and I_{KIR}, differ. The I_{KIR} can rapidly amplify a hyperpolarization, whereas the I_H has a slowly depolarizing effect. The temporal course of these conductances roughly mirrors the resistance change evoked, on depolarization, by the fast depolarizing subthreshold I_{Na} and I_T and the slower hyperpolarizing K^+ currents. The overall increase in conductance results in a decrease in membrane time constant, allowing the

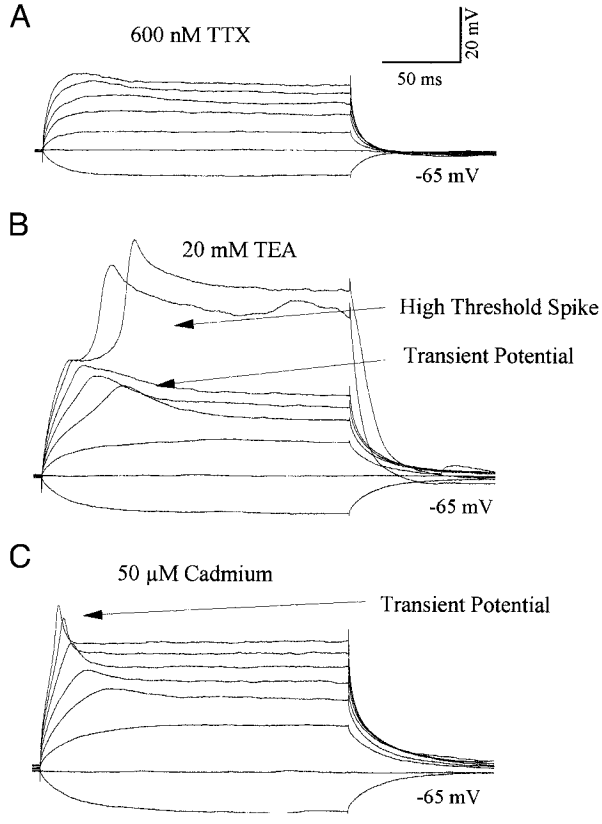

FIG. 13. The HTS and plateau depend on a Cd^{2+}-sensitive Ca^{2+} current. *A*: depolarizing responses were evoked from a membrane potential of -65 mV in the presence of TTX. *B*: addition of 20 mM TEA to the bath enables firing of HTS-plateau complexes. *C*: further addition of 50 μM Cd^{2+} prevents firing of HTSs and plateaus.

cell's membrane potential to change more rapidly. On balance, these nonlinearities may serve to transform coinciding excitatory and inhibitory inputs into an output that provides a linear code for IID within, approximately, the first 50 ms of the stimulus onset. The onset emphasis during both hyperpolarization and depolarization is likely instrumental in the neuronal sensitivity for phase in low-frequency stimuli (Finlayson and Caspary 1991) and amplitude-modulated sounds (Joris 1996; Joris and Yin 1995) found in the LSO.

We demonstrated that a Na^+ conductance and the I_H contribute to the resting membrane potential. It is reasonable to assume that these conductances also are subject to adjustment. For example, the voltage range of activation for I_H typically changes under the influence of neuromodulators such as histamine, acteylcholine, norepinephrine, or glutamate (via metabotropic receptors) (Pape 1996; Santoro et al. 2000). Afferents from the A5 cell group, dorsolateral to the LSO, are thought to release norepinephrine within the LSO, possibly at discrete dendritic sites (Woods and Azeredo 1999; Wynne and Robertson 1996). Glutamate released by ipsilateral afferents also activates metabotropic receptors (Kotak and Sanes 1995). Vesicular acetylcholine transporter (Yao and Godfrey 1998) and choline acetyl transferase are found in puncta within the LSO (Henderson and Sherriff 1991). A cholinergic innervation could be derived from lateral olivocochlear (LOC) neurons (Brown 1993). Here, acetylcholine has been co-localized with other neuromodulators, such as calcitonin gene–related peptide (CGRP), dynorphins, and GABA (Abou-Madi et al. 1987; Altschuler et al. 1984, 1988; Lu et al. 1987; Saffieddine and Eybalin 1992; Schwarz et al. 1988). The RMP can therefore be predicted to change with neuromodulation, possibly affecting the neuron's ability to maintain repetitive firing (Fig. 2). Therefore it will be simplistic to model LSO signaling at one RMP value.

The output of the LSO has been assumed to encode sound direction as firing rate, or as the number of spikes over a time segment. Accordingly, a decaying rate would signal movement of the sound source. To avoid ambiguities between adaptation to a stationary sound stimulus and a moving sound source, an evaluation of rate would have to occur over short time segments. Thus the discharges during the transient potential and its decay may be more important for sound localization than the steady-state firing rate, which, by virtue of its regularity, seems well suited to indicate stability. The LSO output seems to emphasize change over stability: even strong depolarizing current pulses can lead to complete adaptation in firing (Adam et al. 1997). Here, we show that continuous firing strongly depends on the preexisting membrane potential, being maximal during current injection from rest. Currents causing the same depolarization from de- or hyperpolarized prepotentials maintain the onset, but not the steady-state response (Fig. 2). This behavior probably explains why, in vivo, LSO neurons respond with only the onset response to an excitatory stimulus that is preceded by inhibition (Tsuchitani 1988a,b). LSO neurons secure, then, the dynamic onset response under varying conditions, but not the steady-state firing rate. Thus change in stimulus position may be more securely encoded than position itself. In the behaving animal the emphasis of change is reflected in scanning head and pinna movements during precise localization of a stationary sound.

Does the onset response contain sufficient information to encode sound localization? Two parameters in the onset discharge reflect the amplitude of a depolarizing current, and thus possibly, sound source location: *1*) the latency of the first spike and *2*) the initial interspike intervals. In responses to current pulses, the onset spike latency varies systematically with stimulus intensity (Adam et al. 1997) and with the preexisting membrane potential, but over a narrow range (Fig. 2*C*). However, in vivo a wider latency range of the subthreshold transient potential peaks (e.g., Fig. 1) may expand the range of firing latencies, and hence resolution. Separate transient potentials, evoked from numerous excitatory afferents converging onto a pLSO neuron at different dendritic locations, would summate to the extent of their coincidence. For similar reasons, the resolution and range of the first spike interval measure would be greatly enhanced by the effects of convergent excitation, particularly if the subthreshold transient potentials coincide only partially, causing an expansion of transient potential peak duration or even several peaks. The ranges of both onset latency and initial interval would further be widened by the slower onset of naturally occurring EPSPs, compared with current pulses. Thus by virtue of intrinsic properties responsible for the transient potential, principal LSO neurons may be endowed with a dynamic intensity (location) coding capability that has, during the response onset, a far greater resolution in the behaving animal than apparent in vitro in the current pulse response.

In conclusion, the active membrane of pLSO neurons, endowed with the voltage- and time-dependent conductances we have identified (and possibly more), can better account for the firing behavior observed in vivo, including the chopper response, than linear models based on soma-dendritic cable properties. As an added benefit, the corresponding ion channels are, in principle, plastically adjustable, either by changes in expression or by neuromodulation. Without plasticity, the translation of IID into firing rate would produce errors in the code for sound incidence angle as asymmetric hearing losses occur over a lifetime.

This study was supported by the Canadian Institutes for Health Research, the Deafness Research Foundation, and the Rotary Hearing Foundation, Vancouver.

Present address of P. G. Finlayson: Dept. of Otolaryngology, Wayne State University, Lande Building, Rm. 327, 550 E. Canfield, Detroit, MI 48201.

REFERENCES

ABOU-MADI L, PONTAROTTI P, TRAMU G, CUPO A, AND EYBALIN M. Coexistence of putative neuroactive substances in lateral olivocochlear neurons of rat and guinea pig. *Hear Res* 30: 135–146, 1987.

ADAM TJ, SCHWARZ DWF, AND FINLAYSON PG. Firing properties of chopper and delay neurons in the lateral superior olivary nucleus of the rat. *Exp Brain Res* 124: 489–502, 1997.

ALTSCHULER RA, FEX J, PARAKKAL MA, AND ECKENSTEIN F. Co-localization of enkephalin-like and choline acetyl transferase-like immunoreactivities in olivocochlear neurons of the guinea pig. *J Histochem Cytochem* 32: 839–843, 1984.

ALTSCHULER RA, REEKS KA, FEX J, AND HOFFMAN DW. Lateral olivocochlear neurons contain both enkephalin and dynorphin immunoreactivities: immunocytochemical co-localization studies. *J Histochem Cytochem* 36: 797–801, 1988.

ARLE JE AND KIM DO. Neural modeling of intrinsic and spike-discharge properties of cochlear nucleus neurons. *Biol Cybern* 64: 273–283, 1991.

BANKS MI AND SACHS MB. Regularity analysis in a compartmental model of chopper units in the anteroventral cochlear nucleus. *J Neurophysiol* 65: 606–629, 1991.

BOUDREAU JC AND TSUCHITANI C. Binaural interaction in the cat superior olive S segment. *J Neurophysiol* 31: 442–454, 1968.

BROWN MC. Fiber pathways and branching patterns of biocytin-labeled olivocochlear neurons in the mouse brain stem. *J Comp Neurol* 337: 600–613, 1993.

CAIRD D AND KLINKE R. Processing of binaural stimuli by cat superior olivary complex neurons. *Exp Brain Res* 52: 385–399, 1983.

CANT NB AND CASSEDAY JH. Projections from the anteroventral cochlear nucleus to the lateral and medial superior olivary nuclei. *J Comp Neurol* 247: 457–476, 1986.

FINLAYSON PG. Decreased inhibition to lateral superior olive neurons in young and aged Sprague-Dawley rats. *Hear Res* 87: 84–95, 1995.

FINLAYSON PG AND CASPARY DM. Synaptic potentials of chinchilla lateral superior olivary neurons. *Hear Res* 38: 221–228, 1989.

FINLAYSON PG AND CASPARY DM. Low-frequency neurons in the lateral superior olive exhibit phase-sensitive binaural inhibition. *J Neurophysiol* 65: 598–605, 1991.

FINLAYSON PG AND CASPARY DM. Response properties in young and old Fischer-344 rat lateral superior olive neurons: a quantitative approach. *Neurobiol Aging* 14: 127–139, 1993.

GLENDENNING KK, MASTERTON RB, BAKER BN, AND WENTHOLD RJ. Acoustic chiasm. III. Nature, distribution, and sources of afferents to the lateral superior olive in the cat. *J Comp Neurol* 310: 377–400, 1991.

GOLDBERG JM AND BROWN PB. Response of binaural neurons of dog superior olivary complex to dichotic tone stimuli: some physiological mechanisms of sound localization. *J Neurophysiol* 32: 613–636, 1969.

HELFERT RH AND SCHWARTZ IR. Morphological evidence for the existence of multiple neuronal classes in the cat lateral superior olivary nucleus. *J Comp Neurol* 244: 533–549, 1986.

HELFERT RH AND SCHWARTZ IR. Morphologic evidence for the presence of five cell types in the gerbil lateral superior olivary complex. *Brain Res* 6: 269–286, 1987a.

HELFERT RH AND SCHWARTZ IR. Morphological features of five neuronal classes in the gerbil lateral superior olive. *Am J Anat* 179: 55–69, 1987b.

HENDERSON Z AND SHERRIFF FE. Distribution of choline acetyltransferase immunoreactive axons and terminals in the rat and ferret brain stem. *J Comp Neurol* 314: 147–163, 1991.

HEWITT MJ AND MEDDIS R. Regularity of cochlear nucleus stellate cells: a computational modeling study. *J Acoust Soc Am* 93: 3390–3399, 1993.

HUGUENARD JR. Low-threshold calcium currents in central nervous system neurons. *Annu Rev Neurosci* 58: 329–358, 1996.

JORIS PX. Envelope coding in the lateral superior olive. II. Characteristic delays and comparison with responses in the medial superior olive. *J Neurophysiol* 76: 2137–2156, 1996.

JORIS PX AND YIN TCT. Envelope coding in the lateral superior olive. I. Sensitivity to interaural time differences. *J Neurophysiol* 73: 1043–1062, 1995.

KANDLER K AND FRIAUF E. Development of glycinergic and glutamatergic synaptic transmission in the auditory brain stem of perinatal rats. *J Neurosci* 15: 6890–6904, 1995.

KOTAK VC AND SANES DH. Synaptically evoked prolonged depolarizations in the developing auditory system. *J Neurophysiol* 74: 1611–1620, 1995.

LU SM, SCHWEITZER L, CANT NB, AND DAWBURN D. Immunoreactivity to calcitonin gene–related peptide in the superior olivary complex and cochlea of the cat and rat. *Hear Res* 31: 137–146, 1987.

MCCORMICK DA. Functional properties of a slowly inactivating potassium current in guinea pig dorsal lateral geniculate neurons. *J Neurophysiol* 66: 1176–1189, 1991.

MCFARLANE S AND COOPER E. Kinetics and voltage dependence of A-type currents on neonatal rat sensory neurons. *J Neurophysiol* 66: 1380–1391, 1991.

MOORE MJ AND CASPARY DM. Strychnine blocks binaural inhibition in lateral superior olivary neurons. *J Neurosci* 3: 237–242, 1983.

NICHOLS CG AND LOPATIN AN. Inward rectifier potassium channels. *Annu Rev Physiol* 59: 171–191, 1997.

PAPE H-C. Queer current and pacemaker: the hyperpolarization-activated cation current in neurons. *Annu Rev Physiol* 58: 299–327, 1996.

PFEIFFER RR. Classification of response patterns of spike discharges for units in the cochlear nucleus: tone-burst stimulation. *Exp Brain Res* 1: 220–235, 1966.

RALL W. Cable theory for dendritic neurons. In: *Methods in Neural Modeling. From Synapses to Networks*, edited by Koch C and Segev I. Cambridge, MA: MIT Press, 1989, p. 9–62.

RHODE WS, OERTEL D, AND SMITH PH. Physiological response properties of cells labeled intracellularly with horseradish peroxidase in cat ventral cochlear nucleus. *J Comp Neurol* 213: 448–463, 1983.

ROMAND R. Survey of intracellular recording in the cochlear nucleus of the cat. *Brain Res* 148: 43–65, 1978.

SAFFIEDDINE S AND EYBALIN M. Co-expression of NMDA and AMPA/kainite receptor mRNAs in cochlear neurons. *Neuroreport* 3: 1145–1148, 1992.

SANTORO B, SHAN CA, PAVLIDIS LP, SHUMYATSKY G, TIBBS GR, AND SIEGELBAUM SA. Molecular and functional heterogeneity of hyperpolarization-activated pacemaker channels in the mouse CNS. *J Neurosci* 20: 5264–5275, 2000.

SCHEIBEL ME AND SCHEIBEL AB. Neuropil organization in the superior olive of the cat. *Exp Neurol* 43: 337–348, 1974.

SCHWARZ DW, SCHWARZ IE, HU K, AND VINCENT SR. Retrograde transport of [3H]-GABA by lateral olivocochlear neurons in the rat. *Hear Res* 32: 97–102, 1988.

SPANGLER KM, WARR WB, AND HENKEL CK. The projections of principal cells of the medial nucleus of the trapezoid body in the cat. *J Comp Neurol* 238: 249–261, 1985.

STORM JF. Action potential repolarization and a fast afterhyperpolarization in hippocampal neurons. *J Neurophysiol* 385: 733–759, 1987.

STORM JF. Potassium currents in hippocampal pyramidal cells. *Prog Brain Res* 83: 161–187, 1990.

STRÖHMANN B, SCHWARZ DWF, AND PUIL E. Mode of firing and rectifying properties of nucleus ovoidalis neurons in the avian auditory thalamus. *J Neurophysiol* 71: 1351–1360, 1994.

TENNIGKEIT F, SCHWARZ DWF, AND PUIL E. Mechanisms for signal transformation in lemniscal auditory thalamus. *J Neurophysiol* 76: 3597–3608, 1996.

TSUCHITANI C. Discharge patterns of cat lateral superior olivary units to ipsilateral tone-burst stimuli. *J Neurophysiol* 47: 479–500, 1982.

TSUCHITANI C. The inhibition of cat lateral superior olive unit excitatory responses to binaural tone bursts. II. The sustained discharges. *J Neurophysiol* 59: 184–211, 1988a.

TSUCHITANI C. The inhibition of cat superior olivary unit excitatory responses to binaural tone bursts. I. The transient chopper discharges. *J Neurophysiol* 59: 164–183, 1988b.

TSUCHITANI C AND BOUDREAU JC. Single unit analysis of cat superior olive S segment with tonal stimuli. *J Neurophysiol* 29: 684–697, 1966.

ULRICH D AND HUGUENARD JR. Nucleus-specific chloride homeostasis in rat thalamus. *J Neurosci* 17: 2348–2354, 1997.

WOODS CI AND AZEREDO WJ. Noradrenergic and serotoninergic projections to the superior olive: potential for modulation of olivocochlear neurons. *Brain Res* 836: 9–18, 1999.

WU SH AND KELLY JB. Physiological properties of neurons in the mouse superior olive: membrane characteristics and postsynaptic responses studied in vitro. *J Neurophysiol* 65: 230–246, 1991.

WU SH AND KELLY JB. Response of neurons in the lateral superior olive and medial nucleus of the trapezoid body to repetitive stimulation: intracellular and extracellular recordings from mouse brain slice. *Hear Res* 68: 189–201, 1993.

WYNNE B AND ROBERTSON D. Localization of dopamine-beta-hydroxylase–like immunoreactivity in the superior olivary complex of the rat. *Audiol Neurotol* 1: 54–64, 1996.

YAO W AND GODFREY DA. Immunohistochemical evaluation of cholinergic neurons in the rat superior olivary complex. *Microsc Res Tech* 41: 270–283, 1998.

YOUNG ED, ROBERT JM, AND SHOFNER WP. Regularity and latency of units in ventral cochlear nucleus: implications for unit classification and generation of response properties. *J Neurophysiol* 60: 1–29, 1988a.

YOUNG ED, SHOFNER WP, WHITE JA, ROBERT J-M, AND VOIGHT HF. Response properties of cochlear nucleus neurons in relationship to physiological mechanisms. In: *Auditory Function: Neurobiological Bases of Hearing*, edited by Edelman GM, Gall WE, and Cowan WM. New York: Wiley, 1988b, p. 277–312.